JOURNAL OF THERMOPHYSICS AND HEAT TRANSFER
Vol. 22, No. 4, October–December 2008

Adiabatic Two-Phase Flow in Scaled Microchannel Heat Sinks with Cross Links

M. Dang* and I. Hassan†
Concordia University, Montreal, Quebec H3G 1M8, Canada

DOI: 10.2514/1.35954

The effects of cross links, introduced in the channel core of an array of parallel scaled microchannels, were investigated by comparing the flow distribution in six different multichannel configurations. A standard straight channel test section and five other test sections incorporating cross links were used. All test sections had 45 parallel square channels, with a hydraulic diameter of 1.59 mm. The flow distribution was monitored at four select channels. The working mixture was air and water with superficial velocities ranging from 0.03 to 9.93 m/s, and 0.04 to 0.83 m/s, respectively. This corresponds to a range of flow quality between 0 and 0.25, whereby the mass flux range varies from 42 to 834 kg/m^2 · s. It was observed that the cross-linked designs permit fluid communication between channels. Furthermore, the results showed that there is a significant impact on flow distribution when compared with the straight channel design. Flow patterns obtained from flow visualization were presented in terms of fractional time function, and provided further insight into flow characteristics. Compared with a single channel flow regime map, the expected intermittent flow regime was observed 84–90% of the time for the cross-linked designs, and 65–80% of the time for the straight channel design. The effects of cross links on two-phase pressure drop are also documented.

Nomenclature

A	=	cross-sectional area of channel, m^2
D_h	=	hydraulic diameter, $(4A/P)$
Fr	=	Froude number
f	=	fractional time function, $f = N_i/T$
f	=	friction factor
j_G	=	superficial gas velocity, m/s
j_L	=	superficial liquid velocity, m/s
L	=	channel length, m
$\dot{m}_G$	=	mass flow rate of air, kg/s
$\dot{m}_L$	=	mass flow rate of liquid, kg/s
N_i	=	number of observations of a flow configuration
P	=	channel wetted perimeter, m
Re	=	Reynolds number, $(\rho V D_h/\mu)$
S	=	slip ratio, (j_G/j_L)
T	=	total number of observations
V	=	velocity, m/s
W	=	total deviation percentage
We	=	Weber number
X	=	Martinelli parameter
x	=	flow quality, $x = \dot{m}_G/(\dot{m}_G + \dot{m}_L)$
Y	=	mass flow rate percentage of the four selected channels
Z	=	deviation percentage
μ	=	dynamic viscosity, N · s/m^2
ρ	=	density, kg/m^3
Φ^2_{LO}	=	two-phase multiplier

Subscripts

G	=	gas
L	=	liquid
LO	=	all-liquid flow only
GO	=	all-gas flow only
i	=	flow configuration
o	=	outlet
TP	=	two-phase

Received 30 November 2007; revision received 15 May 2008; accepted for publication 16 May 2008.

*Master of Science Student, Department of Mechanical and Industrial Engineering.

†Professor, Department of Mechanical and Industrial Engineering; IbrahimH@alcor.concordia.ca (Corresponding Author).

I. Introduction

IN RECENT years, researchers have been interested in two-phase flow in mini- and microsystems, such as two-phase microchannel heat sinks, which are expected to improve the thermal management capabilities for high-performance miniaturized electronics devices. Since the pioneering work of Tuckerman and Pease [1], many studies have been conducted to investigate heat transfer characteristics in microchannel heat sinks. These studies have advanced the purpose of developing reliable and predictive models for pressure drop and heat transfer in microchannel heat sinks. Improving flow distribution is necessary in an array of parallel channels because maldistribution among channels will lead to poor cooling performance from the nonuniform temperature distribution on the surfaces of heat sinks. For conventional size two-phase heat exchangers, a number of studies have been done to improve flow distribution through header modifications, such as the works of Samson et al. [2], and Hrnjak [3]. Flow distribution can also be improved through modification of the channel core. Some recent studies have considered modification of the channel core by introducing cross-linked channels. These include the works of Jiang et al. [4] and Cho et al. [5] who conducted experiments to compare the performance of cross-linked and standard parallel microchannel heat sinks by applying hot-spot-type heat fluxes. Their results showed that the cross-linked microchannel improved temperature distribution uniformity under specific flow conditions. Both studies recommended that the cross-linked microchannel heat sink configurations should be optimized to handle different cooling demands, heat fluxes, required flow rate, and hot-spot configuration. Dang et al. [6] investigated flow distribution in two scaled microchannel heat sinks which consisted of 45 channels. One differs from the other by the introduction of two cross-linked pathways, which have the same channel width of the standard straight parallel microchannel. There was little difference between the two designs, as they both showed unequal flow distribution. They suggested that more cross links, as well as the larger width of cross links, should be incorporated to investigate the effects of cross links in terms of flow distribution.

The pressure drop and heat transfer characteristics of two-phase flow systems are strongly influenced by the flow patterns. This was recently reconfirmed by Kandlikar [7] when discussing flow boiling

in mini- and microchannels. One of the most important flow patterns linked to flow boiling is the expanding bubble flow pattern, which is characterized by a rapidly growing nucleating bubble which ultimately occupies the entire channel. The rapid expansion of the bubbles is considered as a cause of flow reversal during flow boiling in minichannel and microchannel systems.

Because flow boiling is very complex, flow patterns have been investigated through adiabatic two-phase flow experiments. Much single channel research has been conducted for different shapes, sizes, and working fluids. From these studies, different flow patterns have been observed and generally defined as bubbly flow, stratified flow, plug flow, slug flow, churn flow, and annular flow. A significant number of single channel flow pattern maps have been constructed for a large range of channel sizes. Some of these flow pattern maps can be found in works from Triplett et al. [8], Coleman and Garimella [9], Chung et al. [10], and Hassan et al. [11].

Compared to single channel adiabatic two-phase-flow investigations, limited studies have been made for the flow features in channel array configurations. Recently, Nino et al. [12] conducted visualization experiments in a six-port square channel array of 1.59 mm hydraulic diameter channels with adiabatic two-phase flow of R134A. They presented the fractional time that a flow pattern may exist at a given flow condition, to construct a qualitative flow map for an array of parallel microchannel heat sinks. The fractional time values were defined as the number of observations of a flow configuration divided by the total number of observations at a particular flow condition. Their results showed that the refrigerant flow was distributed evenly throughout the ports for high mass flux and quality conditions, whereas annular flow was a dominant flow regime. They recommended investigating different working fluids to analyze the variation of the fractional time function.

Two-phase pressure drop experiments have been increasingly studied to seek the appropriate two-phase pressure models. The results of two-phase pressure drops were compared with some widely used models, namely, homogeneous, Chisholm [13], Friedel [14], Lee and Lee [15], and Qu and Mudawar [16]. Triplett et al. [8] and Pehlivan [17] showed that their results agreed with those from the homogenous and Chisholm models. However, some other studies showed that these models failed to predict the pressure drop for smaller hydraulic diameters, as shown in the work of Chen et al. [18], when they investigated the pressure drop for two-phase flow in a round copper having an inner diameter of 1.02, 3.17, 5.05, and 7.02 mm. Furthermore, Chung et al. [10] showed that the homogeneous model cannot effectively predict their results of pressure drop in channels with hydraulic diameters of 96 and 100 μm. However, the Lockhart and Martinelli [19] model can sufficiently predict the two-phase frictional pressure drop for their microchannels.

In developing cross-linked heat sinks, a number of unknowns exist, including the width of the cross link and the number of cross-link paths. The present work investigates scaled cross-linked microchannel heat sinks under adiabatic conditions. Experimental data on adiabatic two-phase flow in six different multichannel configurations will be provided. All test sections were designed to monitor flow measurements in four selected channels. The fractional time function is also used in this paper to plot flow patterns versus flow conditions. This provides clarity about the mechanism of flow, as well as flow distribution in an array of parallel microchannels. Moreover, the pressure drop is measured and compared for all test sections, as well as to some of the most widely used models, to gain further insight into the effects of cross links.

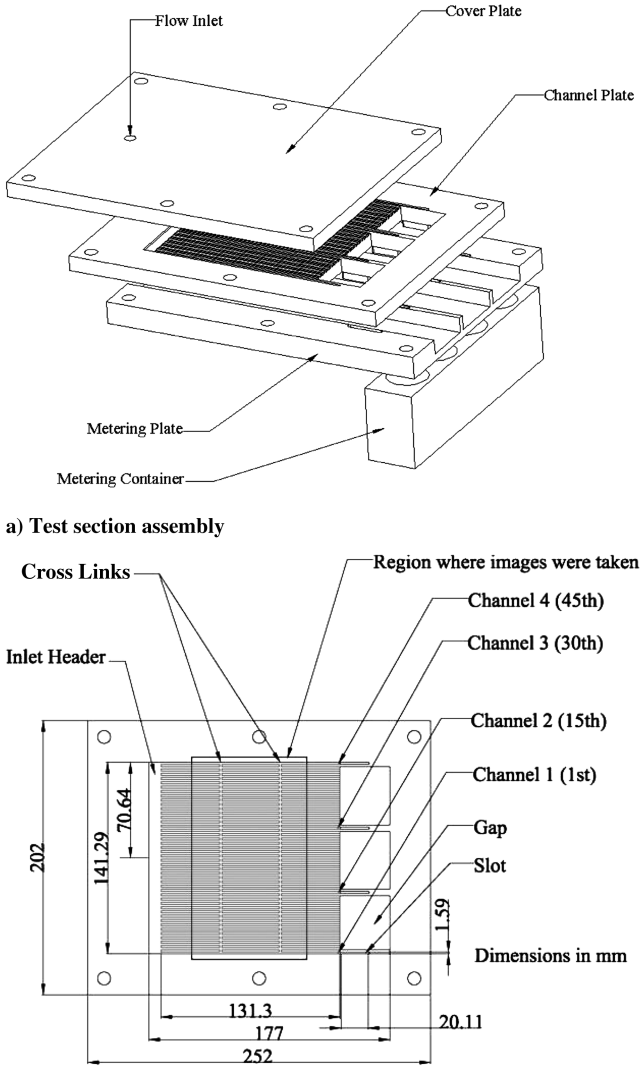

Fig. 1 Test module.

Table 1 Summary of test sections

Test sections	Number of channels	Channel width, mm	Channel length, mm	Number of cross links	Width of cross links, mm	Positions of cross links in respect to channel length
STR	45	1.5875 (1/16 in.)	131.3	——	——	——
CR-2	45	1.5875 (1/16 in.)	131.3	2	1.5875 (1/16 in.)	1/3 and 2/3 s
CR-2A	45	1.5875 (1/16 in.)	131.3	2	3.175 (2/16 in.)	1/3 and 2/3 s
CR-2B	45	1.5875 (1/16 in.)	131.3	2	4.7625 (3/16 in.)	1/3 and 2/3 s
CR-4	45	1.5875 (1/16 in.)	131.3	4	1.5875 (1/16 in.)	1/5, 2/5, 3/5, and 4/5 s
CR-6	45	1.5875 (1/16 in.)	131.3	6	1.5875 (1/16 in.)	1/7, 2/7, 3/7, 4/7, 5/7, and 6/7 s

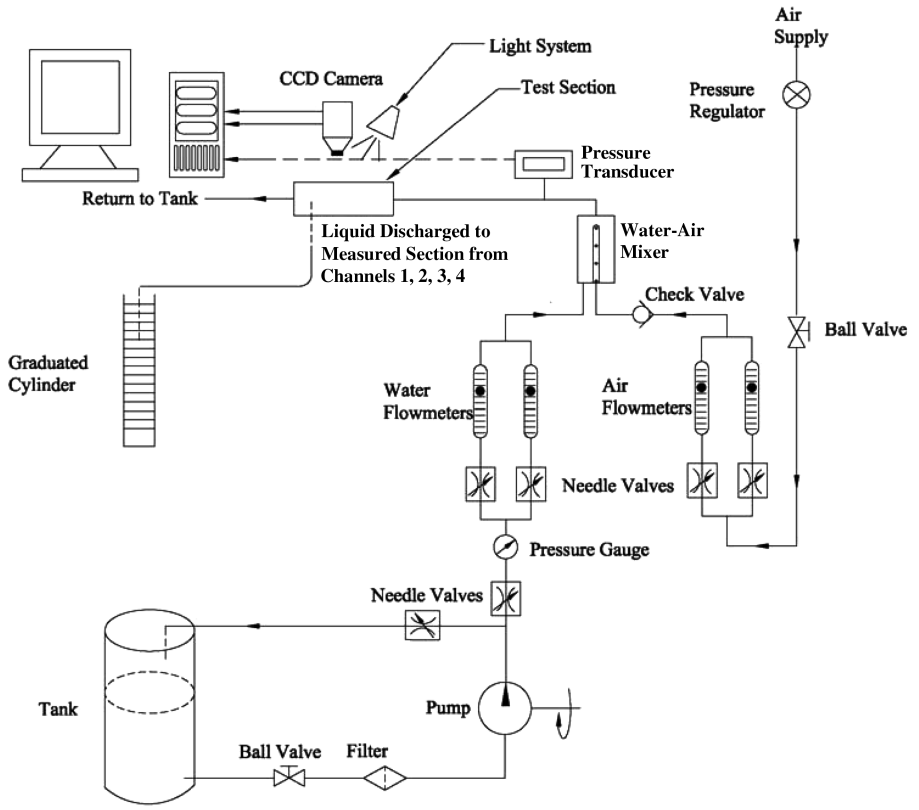

Fig. 2 Schematic drawing of the experimental setup.

II. Experimental Investigation

A. Test Section

The test sections consist of four parts, which are assembled as shown in Fig. 1a. They are a cover plate, a channel plate, a metering plate, and a metering container, in which six different designs of the channel plate are investigated (Fig. 1 and Table 1). Each channel plate was glued with the cover plate to form a multichannel test section. The test sections are a scale up of approximately 9 times the heat sinks used in the work of Muwanga and Hassan [20], and aim to provide rapid and cost effective flow visualization experiments. They are all made from transparent acrylic to facilitate visual access of the flow characteristics. The channel plate consists of a horizontal header with a cross-sectional area of 9×1.59 mm, connected to 45 parallel channels whose cross sections are 1.59×1.59 mm. Four channels, having the same length of 131.3 mm to the other 41 channels, are selected for flow distribution tracking, as shown in Fig. 1b. At the exit of these four channels, the fluid is diverted to metering containers through slots which are open to the atmosphere. A metering plate is used to collect the liquid coming from the remaining channels, whose exits are also open to the atmosphere, and drains them into the reservoir. The inlet hole is located in the middle of the cover plate (Fig. 1a), guiding the two-phase flow into the header of the channel plate. The difference between the six heat sink designs (Table 1) is that the cross links were introduced to the channel core of the standard straight channel test section. The CR-2, CR-2A, and CR-2B test sections consist of two cross links that were located at one-third and two-thirds of the channel length, and their width varied by 1, 2, and 3 times the channel width. Whereby, the CR-4 and CR-6 consist of four and six cross links divided along the channel length into five and seven equal sections, respectively, and their width and height are same as the channel width.

B. Test Facility and Methodology

A schematic of the main components used in the adiabatic two-phase closed-loop test facility is shown in Fig. 2. A 40 liter tank contains distilled water, which is driven through a gear pump with an output of 2.8 l/ min and a maximum pressure of 690 kPa. Two needle valves and a pressure gauge are installed on the delivery line to regulate water to the test section through a set of flow meters,

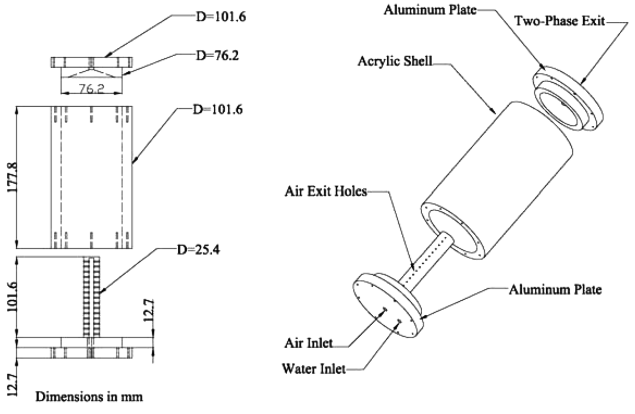

Fig. 3 Mixer assembly.

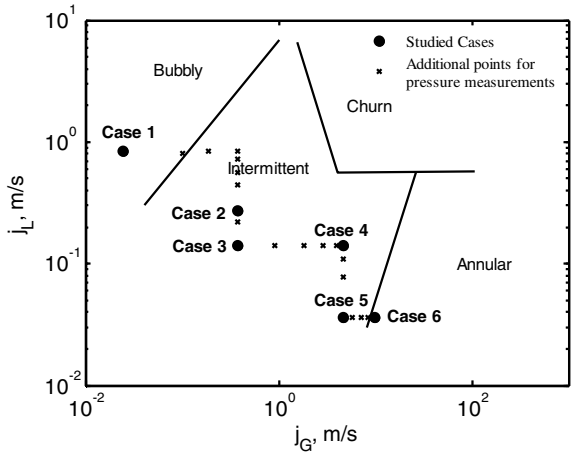

Fig. 4 Simplified flow map, Hassan et al [11].

Table 2 Liquid and gas superficial velocities and flow conditions of the examined flow range

Case	J_G, m/s	J_L, m/s	x	G, kg/m^{2}s
1	0.0245	0.8344	3E–05	834.44
2	0.3777	0.2732	0.0016	273.65
3	0.3777	0.1415	0.0032	141.97
4	4.6044	0.1415	0.0371	146.98
5	4.6044	0.0362	0.1311	41.608
6	9.9259	0.0362	0.2454	47.912

which have a full-scale range of 0.024–7.570 l/ min. Air is supplied with a constant pressure of 724 kPa, and is controlled by a set of flow meters, having a range of 0.01–88 l/ min. The air passes through the check valve, which is used to prevent water backflow into the air line, before entering the mixer. The mixer is vertically installed to assure the two-phase flow is well mixed before entering the test section. The mixer is made of a cylindrically shaped shell with two circular aluminum plates fastened to the ends, as shown in Fig. 3. After the two-phase mixture passes through the test section, the liquid is drained back into the tank to complete the closed-loop liquid circuit. A Sony DXC-9000 3-CCD (charge-coupled device) camera is mounted on the top of the test rig for image capture of the flow inside the channels at a rate of 30 frames/s, and the image acquisition is performed using LabVIEW. A pressure transducer (PX01), ranging from 0–75 psi, is also established between a line connected to the mixer and the test section for pressure measurements. The output of pressure drop measurements is then monitored through an automatic data acquisition system using LabVIEW.

Water is collected from the four selected channels in a graduated cylinder while the elapsed time is recorded (Fig. 2). This procedure is repeated for each of the four selected channels for flow measurements. From uncertainties in the measurement instrumentation, including the timer, flow meters, and metering cylinders, an overall uncertainty of less than 5% is estimated for flow measurements. Surface roughness is not measured before sealing the channels. However, based on the *Machinery's Hand Book* by Oberg et al. [21], the surface roughness is expected to be in the range of 6.3–1.6 μm. Because an image of all four selected channels does not provide a high enough resolution of the flow patterns, images of channels 1 and 2 were taken separately from channels 3 and 4. Flow patterns are analyzed for each of the four selected channels from these images. These flow patterns are then plotted for various flow qualities in terms of a fractional time function f.

Uncertainty in pressure drop measurement is estimated at 0.45 kPa, based on instrument specification. Three sets of 400 data points were taken in 2 s to measure pressure drop for a particular flow condition. The mean of these three measuring sets was calculated for the pressure drop of the system, including the tube connected to the test section. The same procedure was then repeated for the tube only. The pressure drops for the test section are the differences of the means of the preceding pressure drop measurements.

As this work has been carried out in a scaled-up configuration, under adiabatic conditions with an air–water mixture, the applicability of the results to microscale systems needs special

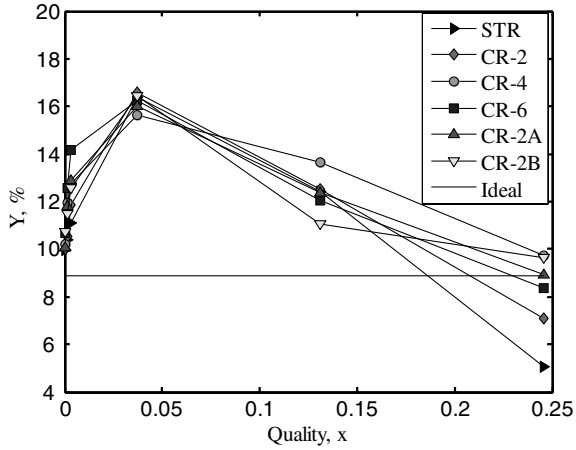

a) Two-phase flow percentage in four selected channel

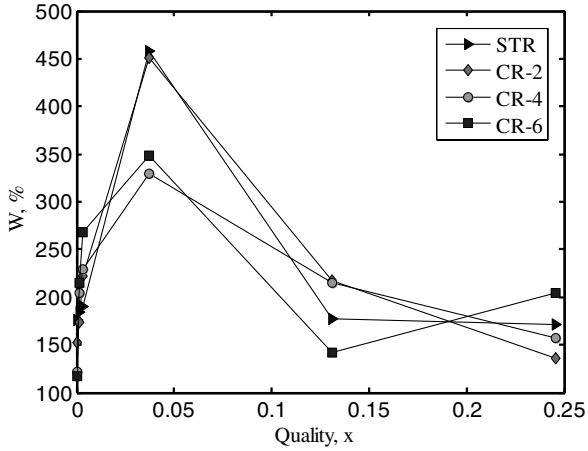

b) The effect of number of cross links

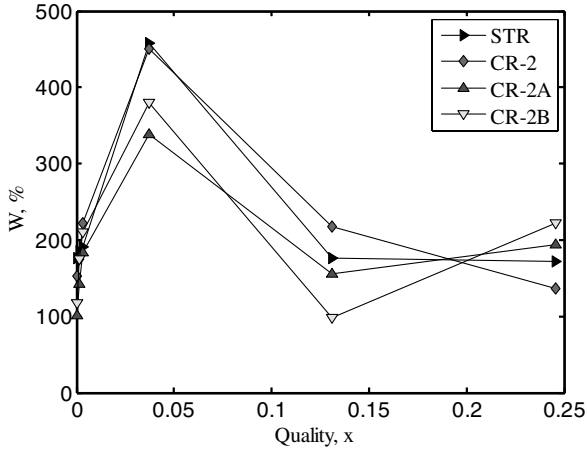

c) The effect of the cross-linked width

Fig. 5 Two-phase flow measurements.

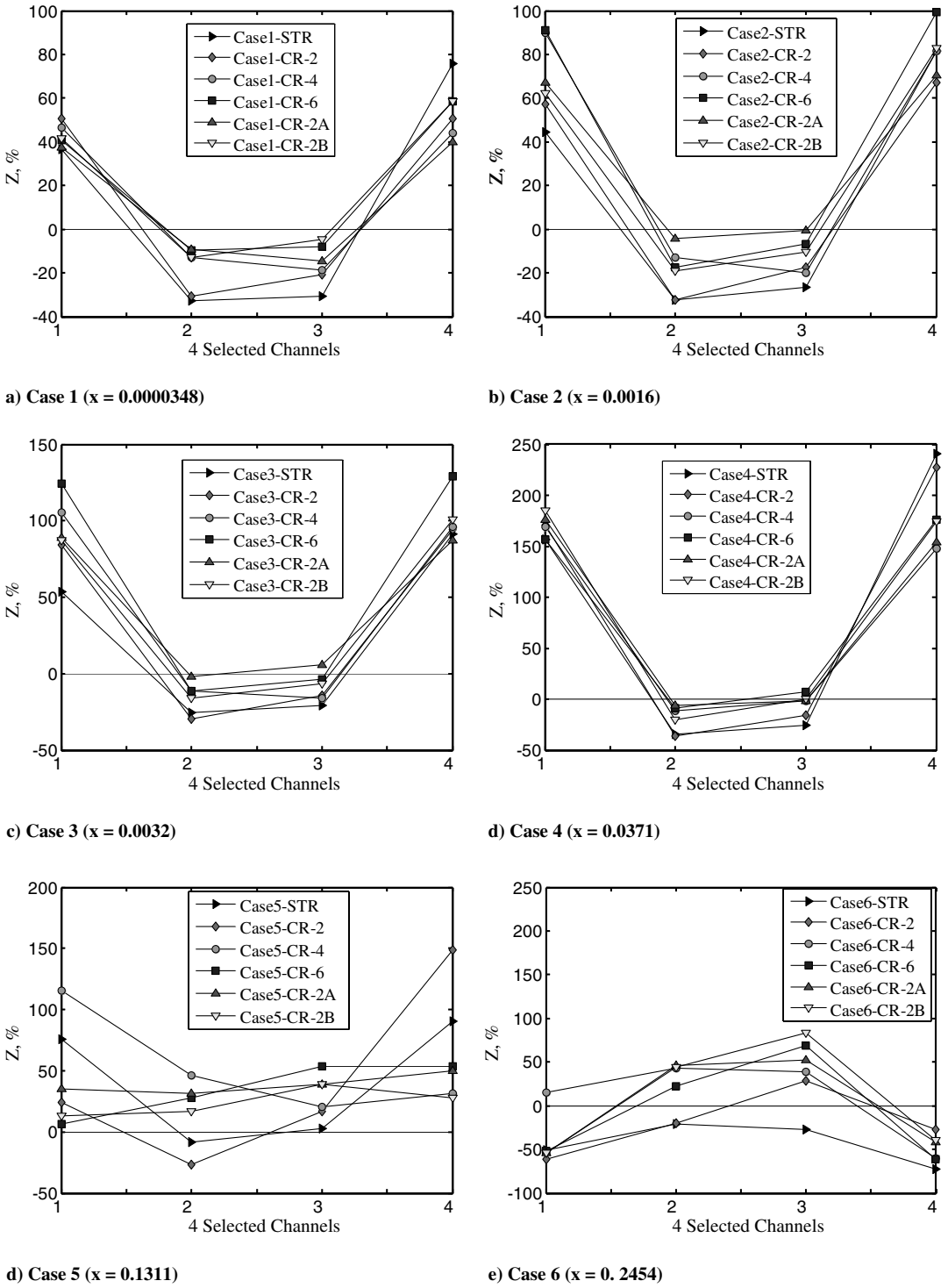

a) Case 1 (x = 0.0000348) **b) Case 2 (x = 0.0016)**

c) Case 3 (x = 0.0032) **d) Case 4 (x = 0.0371)**

d) Case 5 (x = 0.1311) **e) Case 6 (x = 0. 2454)**

Fig. 6 Flow distribution in four selected channels for each studied case.

consideration. A number of nondimensional groups which are relevant to two-phase flow studies in microchannels are listed in the work of Kandlikar [7]. Relevant to the present system is the Weber number We, which represents the ratio of inertia to surface tension forces. The Weber number is considered a useful dimensionless parameter to analyze fluid flows where there is an interface between two different fluids. It may be defined with respect to the hydraulic diameter as $We = G^2 D_h / \rho_{\mathrm{TP}} \sigma$.

Considering the scaling of a system, whereby the two-phase mixture components and the system temperature remain constant, the density and the surface tension, which are fluid properties, will also remain constant. For a fixed Weber number then, reducing the diameter by 9 times in relation to the present work, the mass flux should be increased 3 times. Given the mass flux range examined in the current work (41–834 $\mathrm{kg/m^2 \cdot s}$) and for a fixed Weber number, the results will be applicable in microscale systems of similar two-phase mixture components for a mass flux range of 124–2500 $\mathrm{kg/m^2 \cdot s}$. It is noted that mass fluxes over 1000 $\mathrm{kg/m^2 \cdot s}$ have been used in microsystems, as in the work of Steinke and Kandlikar [22].

III. Results and Discussion

A. Two-Phase Flow Distribution

Two-phase flow measurements were carried out by monitoring the liquid flow from four channels. Six flow conditions (Table 2) were

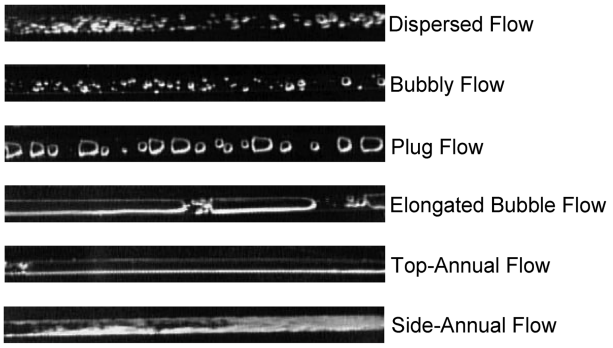

Fig. 7 Samples of flow patterns (direction of flow is from left to right).

examined in the present work, based on the simplified flow map presented by Hassan et al. [11] (Fig. 4), in three different regions, namely bubbly, intermittent, and annular flow regimes. The purpose of choosing these cases is to cover a range of potential flow patterns and to compare flow characteristics between the six test sections presented in this paper.

Figure 5a presents the mass flow rate percentage of the four selected channels. The mass flow rate percentage Y is the ratio of the measured flow in the four selected channels to the total liquid flow rate, whereas the ideal mass flow rate percentage is the ratio of ideal flow, assuming equally distributed flow in all channels. The results vary from 5 to 17% of the total flow, compared with the ideal case of 8.8%. Figures 5b and 5c present flow distribution in terms of the total deviations percentage W in the four selected channels due to the effects of the number and width of cross links. The deviation percentage is defined as the absolute values of the difference in the measured to the ideal flow rate with respect to the ideal flow rate. By definition, the flow distribution would approach uniformity throughout the channels if W moved toward zero. The results show that W is very large and there are no discernible trends between the test sections. The highest deviation occurred for all test sections in case 4 ($x = 0.0371$), whereas the gas flow was significantly increased while the liquid flow remained constant in case 3 (Table 1). High air flow likely drives liquid flow to some of central channels and the outermost channels, such as channels 1 and 4. Hence, high deviation was observed in channels 1 and 4. This high deviation is in part due to entrance effects as the flow is directly injected into the inlet header. This enhances the impact force at the entrance before reaching the inlet of channels. Moreover, the inlet size of channels is small, so that flow is pushed to the ends of the header. However, the results show lower deviations for the CR-4, CR-6, CR-2A, and CR-2B test sections in this case: less than 390% of the deviation for the CR-4, CR-6, CR-2A, and CR-2B test sections compared with over 450% of the deviation in the straight test section (STR) and CR-2 test sections.

Figure 6 presents flow distribution in terms of deviation percentage Z, which is defined in the previous paragraph, from cases 1–6. From cases 1–4, high liquid was observed in channels 1 and 4, which is likely accounted for by the two other channels, 2 and 3, having an opposing trend. Channels 2 and 3 have lower liquid flow in such cases, however, the results show that liquid flow increases in these channels from the cross-linked test sections, compared to that from the straight test section. It is interesting to note that liquid flow is significantly increased in channels 2 and 3 from the CR-2A, CR-2B, and CR-6 test sections, which provide considerably more space for flow sharing along the cross links. Cases 5 and 6 (Figs. 6d and 6e) show that liquid increases in channels 2 and 3, whereas it starts decreasing in channels 1 and 4 for all test sections. This is possibly due to high gas and low liquid flows taken in these two cases, especially in case 6 (Table 1), in which low liquid flow is preferably driven (by air) to channels closed to the inlet. For the STR test section, liquid flow cannot be shared between channels, especially channels 2 and 3. Hence, negative deviations occur in the four selected channels for the STR test section, whereas positive deviation can be observed in these channels for the cross-linked test sections, due to flow sharing between channels through the cross links. In these cases, the cross-linked test sections show better overall flow distribution compared with the straight test section. These cases, however, contain high gas and low liquid flows. It is not recommended to work under these flow conditions if heat is applied to the surface of the heat sinks because a hot spot could occur.

Although the cross-link configurations studied in the current work did not significantly improve the maldistribution caused by the inlet configuration, the influence of cross links on the results of two-phase flow distribution is helpful in seeking promising designs to overcome the entrance effects. As a result, it is proposed that as more cross links are added to the channel core, the flow communicating between channels increases. The larger the width of cross links, the larger the available space in which fluid can communicate. Overall, CR-2A shows better flow distribution in the four selected channels. This will be discussed in depth in the following section of flow visualization.

B. Flow Visualization

The observed flow patterns are described and categorized in accordance with the flow patterns defined by Dang et al. [6]. They are classified into the dispersed, intermittent, and annular flow regimes. The dispersed flow regime is defined as a combination of bubbly flow and dispersed bubbly flow. The intermittent flow regime includes plug flow and elongated bubble flow, whereas the annular flow regime consists of top and side annular flow. These flow patterns are shown in Fig. 7. Figure 8 shows samples of the dominant flow patterns that appeared in the selected channels for some cases. As discussed earlier, more liquid was collected in channels 2 and 3 from the CR-4, CR-6, CR-2A, and CR-2B test sections compared with the STR and CR-2 test sections. This is illustrated in Fig. 8a, which shows that the dominant flow pattern in channel 3 is the elongated flow for the STR and CR-2, whereas plug flow dominates in the same channel for the remaining test sections. Conversely, for case 4, elongated bubble and annular flow are observed in channel 4 for the

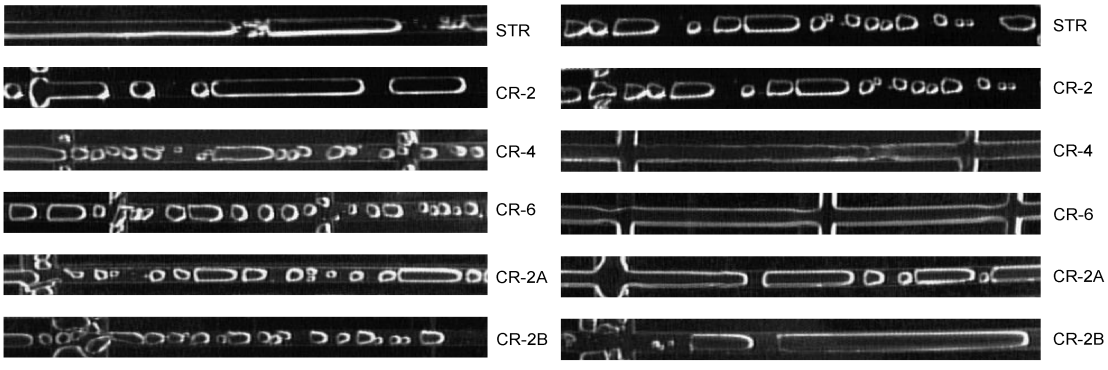

a) Channel 3- case3 **b) Channel 4- case4**

Fig. 8 Samples of flow patterns comparison (direction of flow is from left to right).

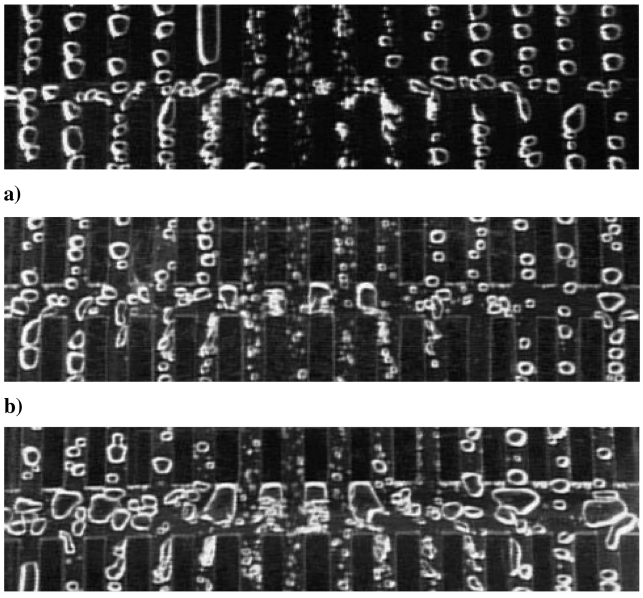

a)

b)

c)

Fig. 9 Samples of flow interaction at case 1: a) CR-2, b) CR-2A, c) CR-2B (direction of flow is from top to bottom).

CR-4, CR-6, CR-2A, and CR-2B test sections, whereas plug flow is observed in this channel for the STR and CR-2 test sections (Fig. 8b). Hence, less liquid was collected in channel 4 for the CR-4, CR-6, CR-2A, and CR_2B test sections than for the STR and CR-2 during case 4. Such results also lead to different flow deviations for all test sections, as discussed in the earlier section, when the cross links are incorporated in the channel core.

The effect of cross links on flow characteristics can be seen in Fig. 9, which presents flow sharing between channels through the cross links. The cross links can be considered as outlet headers, where exit flow in channels can be freely expanded. Hence, flow may be shared with neighboring channels. Bubbles were observed circulating in between channels, especially between two high flow channels. Because these observed bubbles have almost the same size as the size of the cross links (Fig. 9a), this results in less liquid sharing between channels flowpaths. There will be more space for flow communicating as the width of cross links is increased (Figs. 9b and 9c). As a result, more liquid is transferred to some channels, such as channels 2 and 3, from the CR-2A and CR-2B test sections than the remaining test sections (Fig. 5). Larger bubbles were observed to be trapped between channels, which have similar high flow, more so than observed from the CR-2B test section (Fig. 9c). This leads to more liquid collected in channels 2 and 3 from the CR-2A than CR-2B test sections in some particular cases. It can be proposed that increasing the width of the cross links would more successfully increase flow sharing than simply increasing the number of cross links with the same width. Nevertheless, cross links with too large of a width might not be effective, as in the case of the CR-2B test section.

Flow distribution can be better understood when discussing flow patterns. Based on the observed dominant flow patterns, the fractional time functions were constructed for cases 1–4 as shown in Fig. 10. Cases 5–6 are not presented because of the difficulty in distinguishing the gas flow and the annular flow patterns at these high flow qualities. High liquid flow, which was measured in channels 1 and 4, can be explained based on observed flow patterns. Figures 10c and 10d show that no annular flow regime was observed in channels 1

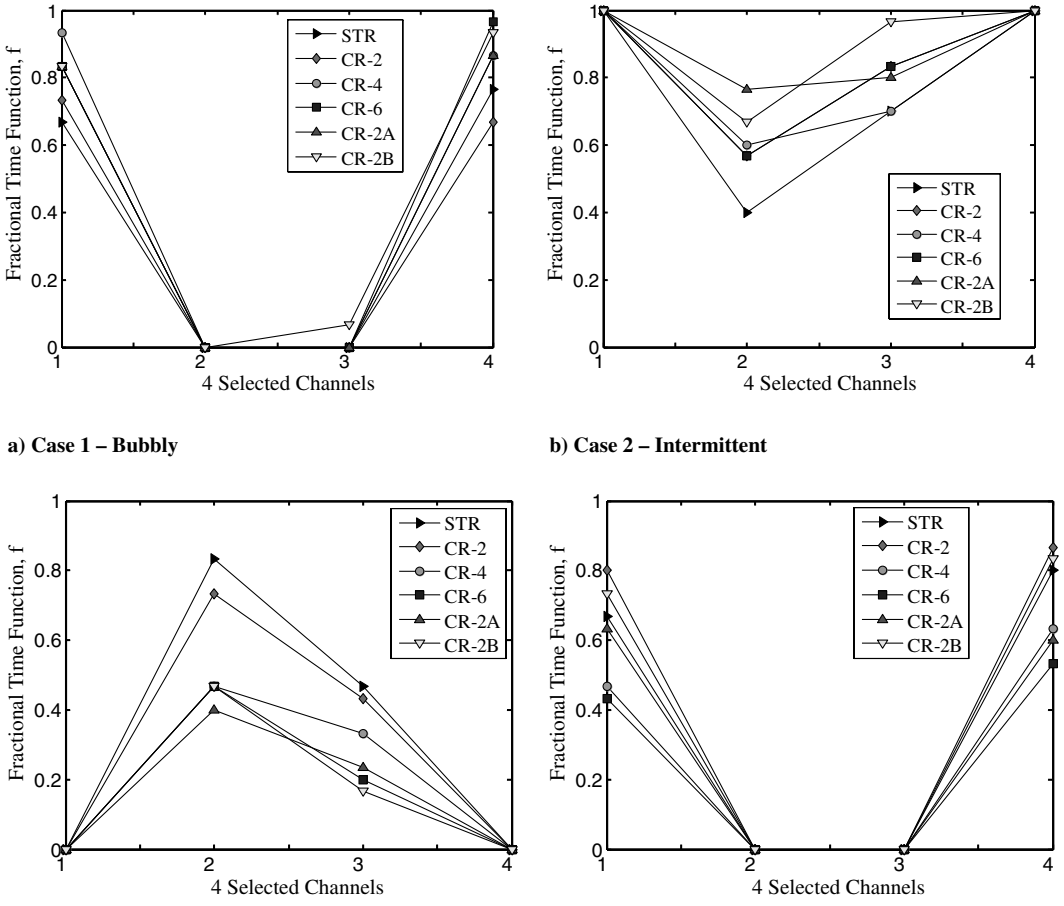

a) Case 1 – Bubbly

b) Case 2 – Intermittent

c) Case 3 – Annular

d) Case 4 – Intermittent

Fig. 10 Fractional flow patterns in particular flow conditions.

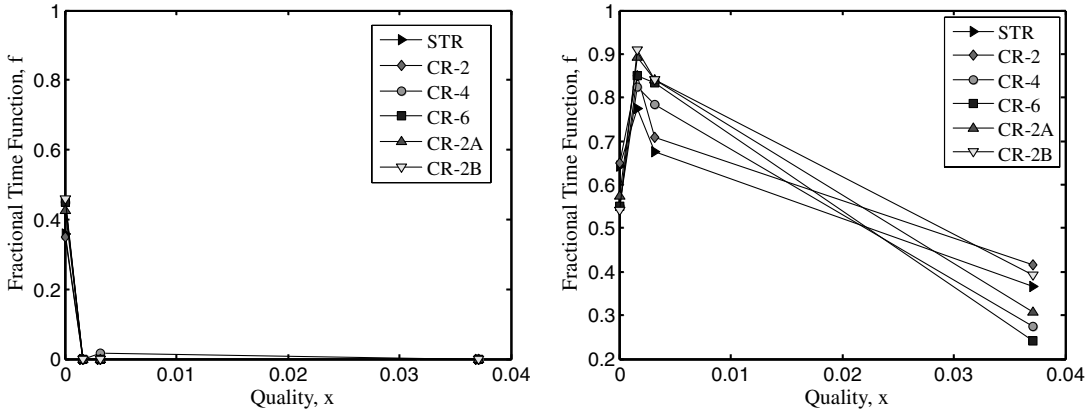

a) Bubbly and dispersed flow

b) Intermittent

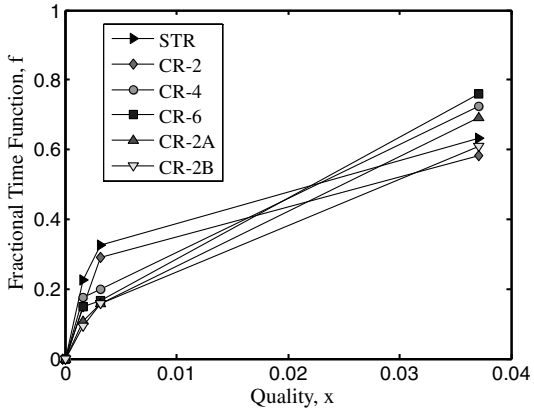

c) Annular flow

Fig. 11 Fractional time flow patterns for four channels of both test sections.

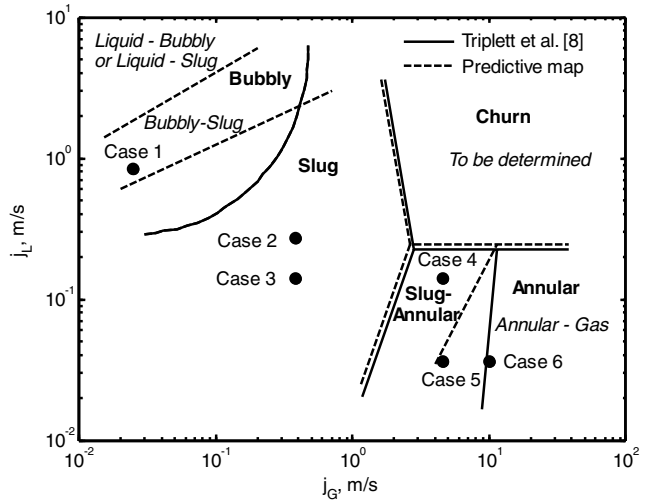

Fig. 12 Dominant flow pattern map, proposed by Dang et al. [6], adapting the single channel flow pattern map of Triplett et al. [8].

and 4 in case 3 ($x = 0.0032$), and no intermittent flow patterns were observed in channels 2 and 3 in case 4 ($x = 0.0371$), the highest deviation case. Noted that there was no bubbly flow observed in four selected channels for these cases. Intermittent flows are lower quality flow patterns than annular flow, and hence more liquid passes when they are present compared with when there is annular flow. It is also seen that more intermittent and less annular flows are observed in channels 2 and 3 for the cross-linked test sections compared with the straight test section. This may be due to flow communication enabled by the cross links breaking up the annular flow pattern. As a result, more liquid was collected in these channels from the cross-linked test sections.

Because there are no appropriate flow maps constructed for multichannel configurations, dominant flow patterns are compared to flow patterns from single channel studies. Figure 11 presents the flow regime in terms of fractional time function for the six test sections, assuming the four selected channels represent the entire test section. The fractional time from these figures is calculated by dividing the number of observations of flow configurations by 120 (30 images $\times$ 4 channels). If the fractional time is equal to 1 at a particular flow condition, it is assumed that the flow is distributed uniformly throughout the channels. Figure 11b shows that the intermittent flow regime for all test sections dominates in case 2 ($x = 0.0016$) and in case 3 ($x = 0.0032$). In these cases, the cross-linked test sections have a higher number of occurrences of this flow regime, from 70 to 90% compared with 65–80% of such observations from the straight design. For other flow regimes, less than 50% of bubbly flow and over 58% of annular flow were observed for all test sections in case 1($x = 0.0000348$) and case 4 ($x = 0.0371$), respectively (Figs. 11a and 11c). Both flow regimes, dispersed and intermittent, are therefore considered as dominant flow regimes in case 1, whereas intermittent and annular are dominant flow regimes in case 4.

The dominant flow patterns observed in the present work are also compared with a multichannel dominant flow pattern map, proposed by Dang et al. [6], adapting a single channel flow pattern map of Triplett et al. [8] (Fig. 12). This two-phase multiple channel flow pattern map was proposed based on a good agreement of Dang et al.'s [6] results of flow patterns when compared with those from the work

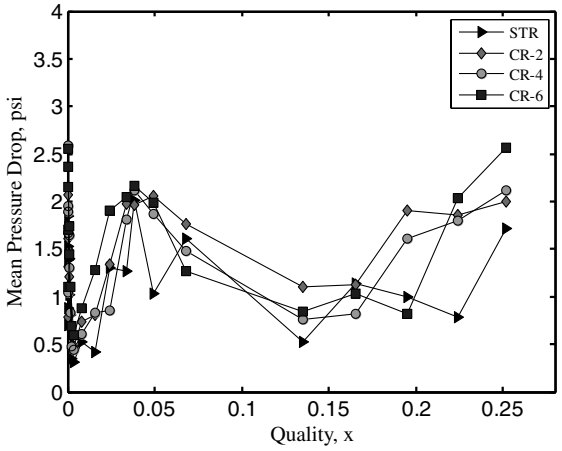

a) Effects of number of cross-links on pressure drop

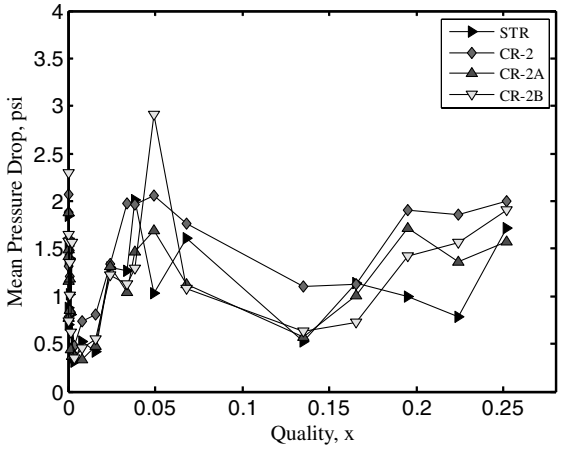

b) Effects of cross-link width on pressure drop

Fig. 13 Two-phase pressure drop comparison.

of Triplett et al. [8] for particular cases 2, 3, and 4. In these cases, slug is the dominant flow pattern in cases 2 and 3, whereas slug–annular flow patterns dominate in case 4. However, bubbly and slug flow are dominant flow patterns in case 1, whereas annular and gas flows are considered as dominant flow patterns in cases 5 and 6. The results show that the proposed map of Dang et al. [6] fairly predict the dominant flow patterns observed in all test sections in the present work. In addition, dominant flow patterns observed in the

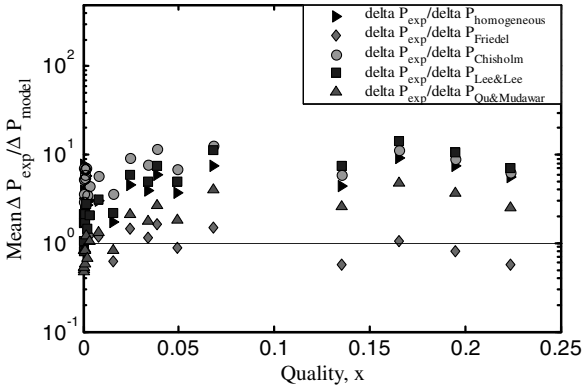

Fig. 14 Pressure drop compared with models from the STR test section.

cross-linked test sections are favorably comparable, whereas there were a higher number of observations of dominant flow patterns compared with those from the straight test section. Dominant flow patterns in the four selected channels could therefore potentially represent the entire channels for all test sections in this work. Further investigation on flow patterns for multiple channels should be made to ascertain the preceding assumptions.

C. Pressure Drop

Two-phase pressure drop, accounting the pressure loss from the tube, is presented in terms of the mean values, as shown in Fig. 13. Figure 13a presents the effect of the number of the cross links on the pressure drop, whereas the effect of the cross-links' width is presented in Fig. 13b. From these figures, the trend of the two-phase pressure drop is discernible for 22 pressure measurements, including six studied cases (Fig. 4). It varies irregularly, up and down, from one to the other within 0–3 psi. To gain further insight into the effects of cross links on pressure drop, the two-phase pressure drop is compared between the test sections in terms of the average deviation percentage. The average deviation percentage is defined as the average value of deviations, accounting for all studied cases. The deviation is the difference of the two-phase pressure drop from two test sections for a particular case. Compared to the straight test section, the average deviations are 41, 45, 65, 24, and 49% for CR-2, CR-4, CR-6, CR-2A, and CR-2B, respectively. The lowest average deviation is observed from the CR-2A test section compared with the straight test section. In addition, the CR-2A test section is considered a better design in terms of flow distribution due to the effectiveness of flow sharing from high flow channels to low flow channels, as discussed earlier. Hence, this design can be considered an approach for further investigation of the effect of cross links, for example,

Table 3 Two-phase pressure drop correlations

Models	Frictional component, ΔP_f
Homogeneous (Collier and Thome [23])	$\Delta P_f = f_{\mathrm{TP}} \frac{L}{D} \frac{\rho_{\mathrm{TP}} U^2}{2}$, where $f_{\mathrm{TP}} = 57/Re_{\mathrm{TP}}$ (laminar), $f_{\mathrm{TP}} = 0.3164\, Re_{\mathrm{TP}}^{-0.25}$ (turbulent), $Re_{\mathrm{TP}} = \frac{\rho_{\mathrm{TP}} UD}{\mu_{\mathrm{TP}}}$, $\rho_{\mathrm{TP}} = [\frac{x}{\rho_G} + (\frac{1-x}{\rho_L})]^{-1}$, $\mu_{\mathrm{TP}} = [\frac{x}{\mu_G} + (\frac{1-x}{\mu_L})]^{-1}$
Friedel [14]	$(-\frac{\mathrm{d}p}{\mathrm{d}z})_{f,\mathrm{TP}} = \Phi_{\mathrm{LO}}^2 (-\frac{\mathrm{d}p}{\mathrm{d}z})_{f,\mathrm{LO}}$, where $(-\frac{\mathrm{d}p}{\mathrm{d}z})_{f,\mathrm{LO}} = \frac{2 f_{\mathrm{LO}} G^2}{D \rho_L}$, $\Phi_{\mathrm{LO}}^2 = A + 3.24 x^{0.78} (1-x)^{0.24} (\frac{\rho_L}{\rho_G})^{0.91} (\frac{\mu_G}{\mu_L})^{0.19} (1 - \frac{\mu_G}{\mu_L})^{0.7}$ $Fr^{-0.0454} We_{\mathrm{TP}}^{-0.035}$, $A = (1-x)^2 + x^2 \rho_L f_{\mathrm{GO}} (\rho_G f_{\mathrm{LO}})^{-1}$, $Fr = \frac{G}{gD\rho_{\mathrm{TP}}^2}$, $We_{\mathrm{TP}} = \frac{G^2 D}{\rho_{\mathrm{TP}} \sigma}$
Chisholm [13]	$(-\frac{\mathrm{d}p}{\mathrm{d}z})_{f,\mathrm{TP}} = \Phi_{\mathrm{LO}}^2 (-\frac{\mathrm{d}p}{\mathrm{d}z})_{f,\mathrm{LO}}$, where $\Phi_{\mathrm{LO}}^2 = 1 + (\frac{C}{X}) + (\frac{1}{X})^2$, ($C = 20$ for turbulent–turbulent, $C = 12$ for laminar–turbulent, $C = 10$ for turbulent–laminar, and $C = 5$ for laminar–laminar), $X^2 = (\frac{\Delta P}{\Delta L})_L / (\frac{\Delta P}{\Delta L})_G$, $Re_L = \frac{G(1-x)D}{\mu_L}$, $Re_G = \frac{G(x)D}{\mu_G}$, $Re_{\mathrm{GO}} = \frac{GD}{\mu_G}$, $Re_{\mathrm{LO}} = \frac{GD}{\mu_L}$
Lee and Lee [15]	$\Delta P_{f,\mathrm{TP}} = \frac{L_{\mathrm{sat}}}{X_o} \int_0^{x_o} \frac{2 f_f G^2 (1-X)^2 \upsilon_L}{D_h} - \Phi_f^2 \, \mathrm{d}x$ $f_f = \frac{24}{Re}(1 - 1.355\beta + 1.947\beta^2 - 1.701\beta^3 + 0.956\beta^4 - 0.254\beta^5)$, $Re_L = \frac{G(1-x)D_h}{\mu_L}$, $Re_G = \frac{GxD_h}{\mu_G}$ $\Phi_f^2 = 1 + \frac{C}{X_{vt}} + \frac{1}{X_{vt}^2}$, $C = 6.185 \times 10^{-2} Re_L^{0.726}$, $X_{vt} = (\frac{f_f Re_G^{0.25}}{0.079})^{0.5} (\frac{1-x}{x})^{0.5} (\frac{\upsilon_L}{\upsilon_G})^{0.5}$ β: aspect ratio
Qu and Mudawar [16]	$\Delta P_{f,\mathrm{TP}} = \frac{L_{\mathrm{sat}}}{x_o} \int_0^{x_o} \frac{2 f_f G^2 (1-x)^2 \upsilon_L}{D_h} \Phi_f^2 \, \mathrm{d}x$ $\Phi_f^2 = 1 + \frac{C}{X_{vv}} + \frac{1}{X_{vv}^2}$, $C = 21(1 - e^{-319 D_h})(0.00418\, G + 0.0613)$ $X_{vv} = (\frac{\mu_L}{\mu_G})^{0.5} (\frac{1-x}{x})^{0.5} (\frac{\upsilon_L}{\upsilon_G})^{0.5}$

changing the position of the cross links or inclining the cross links to the channel core, while keeping the same width of cross links.

Because there are no appropriately experimental studies to be compared with, the present data of the two-phase pressure drop of the straight test section is compared with those calculated from the homogeneous model, and the models by Friedel [14], Chisholm [13], Lee and Lee [15], and Qu and Mudawar [16], as seen in Fig. 14. The homogenous model is one of the simplest models defined for the two-phase pressure drop calculation. This model considers the two phases as a single phase, and assumes that the two phases form a well-mixed mixture. The models of Chisholm [13] and Friedel [14] are separated flow models, assuming liquid and gas flow through different conduits whose areas are proportional to void fraction. These two models use two-phase multiplier Φ^2_{LO}, as expressed in Table 3. The Chisholm model [13] is suggested to be used for $\mu_l/\mu_g > 1000$, whereas the Friedel model [14] is suggested to be used for $\mu_l/\mu_g \ll 1000$ (Whalley [24]). Two recent models, Lee and Lee [15] and Qu and Mudawar [16], incorporating the effects of both channel size and coolant flow rate, are also compared with the present results.

The results show that the average deviation percentages from the present data, obtained from the straight test section to the models of homogeneous, Friedel [14], Chisholm [13], Lee and Lee [15], and Qu and Mudawar [16], are observed as 436, 100, 600, 406, and 111%, respectively. The homogeneous and the Chisholm [13] models underpredict the present data for the whole studied range in the present work. The models of Lee and Lee [15] and Qu and Mudawar [16] fairly predict the present data in some cases, in the low range of quality, but they underpredict when increasing flow quality. The Friedel model [14] underpredicts for the range of case 1–case 2, which is in a very low range of quality, where the bubbly and the plug flows are expected to be minor and major flow patterns, respectively. However, the Friedel model fairly predicts the present data in the range, from the point located just below case 2 to the point which is identical to case 6 (Fig. 4). The range observed covers flow patterns such as plug, elongated bubble, and annular, as discussed in the earlier section. For this range, the average deviation of the present data is observed as 29% compared with the Friedel model, although it is 432, 157, 589, and 685% compared with the homogenous model, and the models of Qu and Mudawar [16], Lee and Lee [15], and Chisholm [13], respectively.

IV. Conclusions

The results of two-phase flow distribution and visualization for six test configurations are presented in this paper. One is a straight standard microchannel heat sink, whereas the rest include cross connections between the channels. The results show that six test sections exhibited nonuniform flow distribution, however, the introduction of cross links to the channel core significantly impacts flow distribution in multiple channels. Three overall conclusions are drawn:

1) The influence of cross-link configurations improves flow distribution compared with the standard straight channel configuration, due to flow sharing along the cross links. The six cross-linked (CR-6), the 2-times larger cross-linked (CR-2A), and the 3-times larger cross-linked (CR-2B) test sections produced better results due to more paths and larger available space for flow in communication. Moreover, the 2-times larger cross-linked test section is considered as an approach design for efficient flow communication through cross links.

2) The dispersed, intermittent (plug, elongated bubble flows), and annular flow regimes were all observed in all six sections. More instances of intermittent flow patterns were observed in the cross-linked test sections, whereas about 90% of intermittent flow patterns were observed from the 2-times and 3-times larger cross-linked test sections. A dominant flow pattern map, adapting a single flow pattern map, fairly predicts dominant flow patterns observed in the present work, whereas dominant flow patterns observed in the cross-linked test sections are favorably comparable.

3) The two-phase pressure drop for the cross-linked test sections deviate discernibly, up and down, when compared with the straight test section. However, the lowest average deviation is observed from the 2-times larger cross-linked test section (CR-2A). The pressure drop model of Friedel [14] fairly predicts the present data from the straight test section in a range that covers plug, elongated, and annular flow patterns.

Flow measurements, pressure measurements, and flow visualization were examined in this paper to gain further insight into the effect of cross links on flow distribution, as well as the flow characteristics in an array of parallel mini- and microchannel heat sinks. The results provide significant data in investigating the effect of cross links introduced to the channel core of parallel multichannel systems.

References

[1] Tuckerman, D. B., and Pease, R. F. W., "High-Performance Heat Sinking for VLSI," *Electron Device Letters*, Vol. 2, No. 5, 1981, pp. 126–129. doi:10.1109/EDL.1981.25367

[2] Samson, E. B., Stark, J. A., and Grote, M. G., "Two-Phase Flow Header Tests," *17th Intersociety Conference on Environmental Systems*, Society of Automotive Engineers Technical Paper Series, Society of Automotive Engineers, Warrendale, PA, p. 19, 1987.

[3] Hrnjak, P., "Developing Adiabatic Two-Phase Flow in Headers: Distribution Issue in Parallel Flow Microchannels Heat Exchangers," *Heat Transfer Engineering*, Vol. 25, No. 3, 2004, pp. 61–68. doi:10.1080/01457630490280128

[4] Jiang, L., Koo, J. M., Wang, E., Bari, A., Cho, E. S., Ong, W., Prasher, R. S., Maveety, J., Kim, M. S., Kenny, T. W., Santiago, J. G., and Goodson, K. E., "Cross-Linked Microchannels For VLSI Hotspot Cooling," *ASME International Mechanical Engineering Congress and Exposition*, American Society of Mechanical Engineers, Fairfield, NJ, 2002, pp. 13–17.

[5] Cho, E. S., Koo, J., Jiang, L., Prasher, R. S., Kim, M. S., Santiago, J. G., Kenny, T. W., and Goodson, K. E., "Experimental Study on Two-Phase Heat Transfer in Microchannel Heat Sinks with Hotspots," *Annual IEEE Semiconductor Thermal Measurement and Management Symposium*, Inst. of Electrical and Electronic Engineers, New York, 2003, pp. 242–246.

[6] Dang, M., Hassan, I., and Muwanga, R., "Adiabatic Two-Phase Flow Characteristics in Scaled Microchannel Heat Sinks," *Experiments in Fluids*, Vol. 43, No. 6, 2007, pp. 873–885. doi:10.1007/s00348-007-0351-x

[7] Kandlikar, S. G., "Effect of Liquid-Vapor Phase Distribution on the Heat Transfer Mechanisms During Flow Boiling in Minichannels and Microchannels," *Heat Transfer Engineering*, Vol. 27, No. 1, 2006, pp. 4–13. doi:10.1080/01457630500341607

[8] Triplett, K. A., Ghiaasiaan, S. M., Abdel-Khalik, S. I., and Sadowski, D. L., "Gas-Liquid Two-Phase Flow in Microchannels, Part 1: Two-Phase Flow Patterns," *International Journal of Multiphase Flow*, Vol. 25, No. 3, 1999, pp. 377–394. doi:10.1016/S0301-9322(98)00054-8

[9] Coleman, J. W., and Garimella, S., "Characterization of Two-Phase Flow Patterns in Small Diameter and Rectangular Tubes," *International Journal of Heat and Mass Transfer*, Vol. 42, No. 15, 1999, pp. 2869–2881. doi:10.1016/S0017-9310(98)00362-7

[10] Chung, P. M.-Y., Kawaji, M., Kawahara, A., and Shibata, Y., "Two-Phase Flow Through Square and Circular Microchannels: Effects of Channel Geometry," *Transactions of the ASME*, Vol. 126, No. 4, 2004, pp. 546–552. doi:10.1115/1.1777580

[11] Hassan, I., Vaillancourt, M., and Pehlivan, K., "Two-Phase Flow Regime Transition in Microchannels: A Comparative Experimental Study," *Microscale Thermophysical Engineering*, Vol. 9, No. 2, 2005, pp. 165–182. doi:10.1080/10893950590945049

[12] Nino, V. G., Hrnjak, P. S., and Newell, TY. A., "Two-Phase Flow Visualization of R134A in a Multiport Microchannel Tube," *Heat Transfer Engineering*, Vol. 24, No. 1, 2003, pp. 41–52. doi:10.1080/01457630304042

[13] Chisholm, D., "Theoretical Basis for the Lockhart Martinelli Correlation for Two-Phase Flow," *International Journal of Heat and Mass Transfer*, Vol. 10, No. 12, 1967, pp. 1767–1778. doi:10.1016/0017-9310(67)90047-6

[14] Friedel, L., "Improved Friction Pressure Drop Correlations for

Horizontal and Vertical Two-Phase Pipe Flow," *European Two-Phase Group Meeting*, Joint Research Center, European Commission Paper E2, 1979.

[15] Lee, H. J., and Lee, S. Y., "Pressure Drop Correlations for Two-Phase Flow Within Horizontal Rectangular Channels with Small Heights," *International Journal of Multiphase Flow*, Vol. 27, No. 5, 2001, pp. 783–796. doi:10.1016/S0301-9322(00)00050-1

[16] Qu, W., and Mudawar, I., "Measurement and Prediction of Pressure Drop in Two-Phase Micro-Channel Heat Sinks," *International Journal of Heat and Mass Transfer*, Vol. 46, No. 15, 2003, pp. 2737–2753. doi:10.1016/S0017-9310(03)00044-9

[17] Pehlivan, K. K., "Experimental Study on Two-Phase Flow Regimes and Fractional Pressure Drop in Mini- and Micro-Channels," M.S. Thesis, Concordia Univ., Montreal, 2003.

[18] Chen, I. Y., Yang, K. S., Chang, Y. J., and Wang, C. C., "Two-Phase Pressure Drop of Air-Water and R-410A in Small Horizontal Tubes," *International Journal of Multiphase Flow*, Vol. 27, No. 7, 2001, pp. 1293–1299. doi:10.1016/S0301-9322(01)00004-0

[19] Lockhart, R. W., and Martinelli, R. G., "Proposed Correlations for Isothermal Two-Phase Two-Component Flow in Pipes," *Chemical Engineering Progress*, Vol. 45, 1949, pp. 39–48.

[20] Muwanga, R., and Hassan, I., "Flow Boiling Oscillations in Microchannel Heat Sinks," *9th AIAA/ASME Joint Thermophysics and Heat Transfer Conference*, AIAA, Reston, VA, 2006, p. 11.

[21] Oberg, E., Jones, F. D., Horton, H. L., and Ryffell, H. H., *Machinery's Handbook*, 26th ed., Industrial Press, New York, 2000.

[22] Steinke, M. E., and Kandlikar, S. G., "Experimental Investigation of Flow Boiling Characteristics of Water in Parallel Microchannels," *Transactions of the ASME*, Vol. 126, No. 4, 2004, pp. 518–526. doi:10.1115/1.1778187

[23] Collier, J. G., and Thome, J. R., *Convective Boiling and Condensation*, 3rd ed., Oxford Univ. Press, Oxford, England, U.K., 1994.

[24] Whalley, P. B., *Boiling, Condensation and Gas–Liquid Flow*, Oxford Univ. Press, New York, 1987.